
Enhancing Exploration in Global Optimization by Noise Injection in the Probability Measures Space

Gaëtan Serré^{1†} Pierre Germain^{23†} Samuel Gruffaz^{1†} Argyris Kalogeratos¹

Abstract

McKean-Vlasov (MKV) systems provide a unifying framework for recent state-of-the-art particle-based methods for global optimization. While individual particles follow stochastic trajectories, the probability law evolves deterministically in the mean-field limit, potentially limiting exploration in multimodal landscapes. We introduce two principled approaches to inject noise directly into the probability law dynamics: a perturbative method based on conditional MKV theory, and a geometric approach leveraging tangent space structure. While these approaches are of independent interest, the aim of this work is to apply them to global optimization. Our framework applies generically to any method that can be formulated as a MKV system. Extensive experiments on multimodal objective functions demonstrate that both our noise injection strategies enhance consistently the exploration and convergence across different configurations of dynamics, such as Langevin, Consensus-Based Optimization, and Stein Boltzmann Sampling, providing a versatile toolkit for global optimization.

1. Introduction

Global optimization aims at finding the global minimum x^* of a non-convex function V (Pintér, 1996; Lee et al., 2017; Awasthi et al., 2024; Houssein et al., 2024; El Yadari et al., 2024; Franceschi et al., 2024). While deterministic optimization methods, such as the ubiquitous gradient descent, are efficient for convex problems, they often get trapped in local minima when the function landscape is non-convex. A

[†]Equal contribution ¹Université Paris-Saclay, ENS Paris-Saclay, CNRS, Centre Borelli, 91190 Gif-sur-Yvette, France

²École des Ponts ParisTech, Marne-la-Vallée, France ³University of Neuchâtel, Neuchâtel, Switzerland. Correspondence to: Pierre Germain <pierre.germain@unine.ch>, Gaëtan Serré <gaetan.serre@ens-paris-saclay.fr>, Samuel Gruffaz <samuel.gruffaz@ens-paris-saclay.fr>.

Preprint. February 2, 2026.

natural approach is to introduce randomness, which forces the optimization algorithm to explore the search space and escape suboptimal solutions.

In finite dimensions, a successful strategy combines randomness with stochastic dynamics via the Langevin equation:

$$dX_t = -\nabla V(X_t)dt + \sqrt{2\kappa}dB_t, \quad (1)$$

where $\kappa \geq 0$ controls the noise intensity and B_t is a standard Brownian motion (Roberts & Tweedie, 1996). Under mild conditions, the distribution ρ_t of X_t converges to the Gibbs measure $\rho_\kappa(dx) \propto \exp(-V(x)/\kappa)$ related to potential V , which concentrates near global minima for appropriate choice of κ . Moreover, the evolution $t \mapsto \rho_t$ corresponds to the gradient flow of the free energy functional $\mathcal{F}_\kappa(\rho) = \text{KL}(\rho \parallel \rho_\kappa)$ in Wasserstein space. Convergence to ρ_κ requires either very large time or high temperature κ . However, increasing κ to speed up convergence has a downside: it spreads ρ_κ out rather than concentrating it on the set of global minimizers X^* . To adaptively manage this trade-off, a scheduler for gradually decreasing the temperature is necessary to achieve both rapid convergence and concentration of the limiting measure on X^* . Simulated annealing has broadly exemplified this approach.

McKean-Vlasov systems. To balance exploration and exploitation more effectively, modern algorithms employ multiple interacting particles with different initializations. These methods, ranging from heuristic approaches to principled gradient flows on probability spaces, can be formulated as instances of McKean-Vlasov (MKV) systems:

$$dX_t^i = b(X_t^i, \hat{\rho}_{X_t})dt + \sigma(X_t^i, \hat{\rho}_{X_t})dB_t^i, \quad (2)$$

where $\hat{\rho}_{X_t}$ is the empirical distribution of all N particles at time t , and $(B_t^i)_{i \geq 1}$ are independent Brownian motions. The drift b and diffusion σ coefficients, which depend on the particle distribution, induce particle interactions that promote both exploration and exploitation. This general framework unifies several recently proposed methods: Consensus-Based Optimization (CBO) (Pinnau et al., 2017) and Stein Boltzmann Sampling (SBS) (Serré et al., 2025) are both special instances of Eq. 2 with specific choices of b and σ . We refer the reader to Appendix C for a detailed introduction to stochastic differential equations and MKV theory.

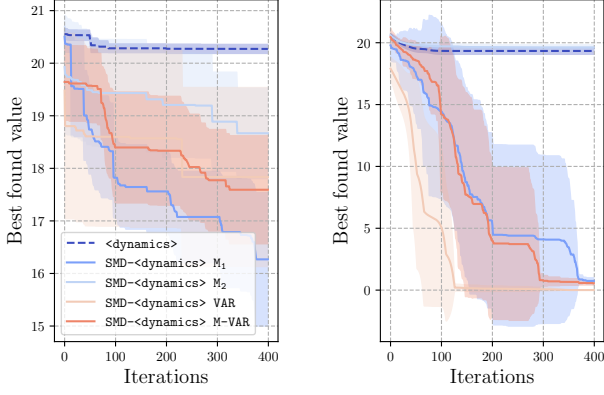


Figure 1. Impact of perturbed observables on CBO (left) and multi-start gradient descent dynamics (right) on Ackley function in dimension 4 with 30 particles. The mean (line) and standard deviation (shaded area) of the best found value are reported over 5 runs.

In the mean-field limit as $N \rightarrow \infty$, the empirical distribution $\hat{\rho}_{X_t}$ converges to a deterministic probability law ρ_t , reducing the system to deterministic mean-field dynamics. The convergence of ρ_t to a measure supported on X^* is then studied (e.g. (Koß et al., 2024; Fornasier et al., 2024; Serré et al., 2025)), with the Gibbs measure being a canonical example (Hwang, 1980). However, this deterministic evolution of ρ_t , arising from averaging independent Brownian motions, potentially limits exploration at the population level, causing the dynamics to fail at exploring multiple modes of complex landscapes and to get trapped in suboptimal basins.

Noise as a plug-in component. To address this limitation, we adopt a distinctive modular perspective: we treat noise as a separate component that can be incorporated to any instance of MKV dynamics. We develop two principled recipes for injecting noise directly into the probability law evolution itself, that we call ρ -noise for the sake of conciseness and consistency. The first approach stems from Germain & Monmarché (2025); it relies on Conditional MKV theory and adds finite-dimensional common noise designed so that key observables (mean, variance) follow a prescribed stochastic evolution. This correlated motion enables collective transitions and facilitates the exploration of multiple basins of attraction. The second approach, novel to this work, leverages the geometric structure of probability spaces by introducing noise in the tangent space of the probability law manifold. This modular approach allows our noise injection strategies to be applied generically to any MKV-based method, treating noise enhancement as a plug-in module that is independent of the underlying dynamics.

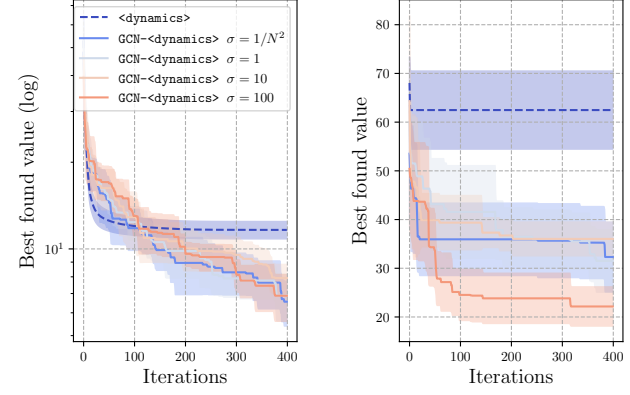


Figure 2. Impact of σ on the RKHS noise for the SBS dynamics (left) and the CBO dynamics (right) on the Levy function in dimension 10 with 10 particles. The mean (line) and standard deviation (shaded area) of the best found value are reported over 5 runs.

Contributions. Being the first to use ρ -noise for global optimization, this paper makes the following main contributions:

- **Two principled approaches for injecting noise** into MKV probability law dynamics: (i) an application of the perturbation-based method of Germain & Monmarché (2025), namely *Stochastic Moment Dynamics* (SMD), to d -dimensional observables; and (ii) *Geometric Common Noise* (GCN), a novel geometric approach that exploits the tangent-space structure of probability measure spaces to induce Langevin-type dynamics at the level of probability laws.
- **Comprehensive experimental validation** across multiple MKV dynamics (Langevin, Consensus-Based Optimization, Stein Boltzmann Sampling, and MSGD) and 7 multimodal benchmark functions, showing that common noise substantially improves exploration and convergence compared to vanilla methods, opening new avenues for both global optimization and sampling applications.

Notations. The finite set $\{1, \dots, N\}$ is denoted by $[N]$. The pushforward of a measure is denoted by $\#$, i.e. $f \# \nu(A) = \nu(f^{-1}(A))$ for any measurable function $f : (\mathcal{X}, \mathcal{B}) \rightarrow (\mathcal{Y}, \mathcal{A})$, $A \in \mathcal{A}$ (σ -algebra on \mathcal{Y}) and ν a measure on $(\mathcal{X}, \mathcal{B})$. We denote by $k_\sigma^{(d)}(x, y) := \exp(-\|x - y\|_2^2/\sigma)$ the Gaussian kernel for any $(x, y) \in (\mathbb{R}^d)^2$ and $\sigma > 0$. \mathcal{S}_d^{++} is the set of d -square symmetric positive definite matrices.

2. Preliminaries

Recent advances in global optimization have been driven by MKV-type algorithms, which represent the state-of-the-art for particle-based methods. These approaches leverage

interacting particle systems that evolve according to mean-field dynamics, and enable effective exploration of complex multimodal objective functions.

In this work, we consider a modular view over MKV dynamics, in which noise injection can be handled by a generic plug-in component, regardless the specifics of a method’s dynamics. Next, we introduce key MKV-based algorithms that have demonstrated superior performance on challenging optimization tasks and are candidates for incorporating our noise injection mechanisms. This diverse list also justifies the broad impact of our approach.

■ **MSGD** $(b, \sigma) = (-\nabla V, 0)$. Multi-start gradient descent (MSGD) is a widely used baseline for global optimization, where multiple particles are initialized randomly and updated via gradient descent.

■ **Langevin** $(b, \sigma) = (-\nabla V, \sqrt{2\kappa}I_d)$, $\kappa > 0$. The Langevin dynamics is a stochastic optimization method that combines gradient descent with isotropic Brownian noise.

■ **SBS** $(b, \sigma) = (b^{\text{svgd}}, 0)$. Stein Boltzmann Sampling (SBS) (Serré et al., 2025) is a particle-based optimization method that leverages repulsive forces $\nabla_x k(\cdot, x)$ between particles to enhance exploration, the drift term is defined as follows

$$b^{\text{svgd}}(\cdot, \rho) \stackrel{\text{def}}{=} \mathbb{E}_{x \sim \rho} \left[-k(\cdot, x) \nabla V(x) + \kappa \nabla_x k(\cdot, x) \right] \quad (3)$$

where $\kappa > 0$ is a temperature parameter and k is a positive definite kernel, typically chosen as a Gaussian kernel. It is based on Stein Variational Gradient Descent (SVGD), which is originally a sampling method derived from the gradient flow of the free energy functional \mathcal{F}_κ in the Stein geometry framework (Duncan et al., 2023). In Section 3.2, we build on this observation to design a ρ -noise that we believe to be canonical.

■ **CBO** $(b, \sigma) = (b^{\text{CBO}}, \sigma^{\text{CBO}})$. Consensus-Based Optimization (CBO) (Pinnau et al., 2017) is a popular particle-based optimization method that drives particles towards a consensus point computed as a weighted average of the best-performing particles. The resulting MKV system has drift and diffusion terms given respectively by:

$$\begin{aligned} b^{\text{CBO}}(X_t^i, \hat{\rho}_{X_t}) &\stackrel{\text{def}}{=} -\lambda(X_t^i - v_f) H^\varepsilon(f(X_t^i) - f(v_f)) \\ \sigma^{\text{CBO}}(X_t^i, \hat{\rho}_{X_t}) &\stackrel{\text{def}}{=} \gamma \|X_t^i - v_f\|_2 I_d, \end{aligned}$$

where H^ε is a smooth approximation of the Heaviside function, $\lambda, \gamma > 0$ are hyperparameters, and v_f is the consensus point defined as:

$$v_f \stackrel{\text{def}}{=} \frac{\sum_{i=1}^N X_t^i e^{-\alpha f(X_t^i)}}{\sum_{i=1}^N e^{-\alpha f(X_t^i)}},$$

where $\alpha > 0$ is a weighting parameter corresponding to the inverse temperature in a Gibbs measure. While anisotropic

noise variants of CBO have been proposed (Carrillo et al., 2021) that could extend this list, we focus on the original isotropic formulation for straightforward compatibility with the MKV framework.

3. Methodology

First, we present an ad hoc finite-dimensional ρ -noise, called SMD, introduced in (Germain & Monmarché, 2025) (Section 3.1). We then introduce an infinite-dimensional ρ -noise, which we claim is canonical when the MKV equation is derived from a gradient flow (Section 3.2).

3.1. Noise through moment perturbation

Mean-field optimization and particle systems. Particle-based optimization methods (Pinnau et al., 2017; Serré et al., 2025; Roberts & Tweedie, 1996) can be viewed as evolutions in the space of probability measures, approximated by interacting particle systems. When particles are driven only by independent noise, stochasticity vanishes in the mean-field limit due to propagation of chaos, often resulting in poor exploration and convergence to local minima (Tugaut, 2014; Monmarché & Reyner, 2025).

Common noise and conditional MKV theory. A natural remedy is to introduce a *common noise* that acts on all particles simultaneously. Unlike independent noise, common noise persists in the mean-field limit and induces ‘genuinely’ stochastic dynamics for the limiting distribution. This setting, known as *conditional McKean–Vlasov theory* (Carmona & Delarue, 2018), has recently been used to improve exploration (Delarue & Vasileiadis, 2025), escape local minima (Delarue et al., 2024; Maitre, 2023), and design structured perturbations (Delarue & Hammersley, 2025). It is particularly motivated by two failure modes: particle collapse (vanishing variance) and collective trapping in suboptimal basins.

Macroscopic perturbations via stochastic moments. To address these issues, one can perturb directly macroscopic observables (e.g. the empirical mean or variance). This is achieved by augmenting the mean-field dynamics with a suitably designed common noise so that the induced evolution of these moments remains stochastic in the mean-field limit. The resulting ρ -noise, termed *Stochastic Moment Dynamics* (SMD), was introduced in Germain & Monmarché (2025) for general observables, together with a theoretical analysis. Here, we provide a self-contained presentation of the method, with a focus on practical implementation.

Macroscopic observable of interest F . Let $N \geq 1$, starting from the baseline mean-field particle dynamics Eq. 2, choose a macroscopic observable $F : \mathcal{P}(\mathbb{R}^d) \rightarrow \mathbb{R}^p$ from:

- Mean: $F_{\text{mean}}(\rho) \stackrel{\text{def}}{=} \int_{\mathbb{R}^d} x d\rho(x)$
- Second-order moment: $F_{\text{s.m.}}(\rho) \stackrel{\text{def}}{=} \left(\int_{\mathbb{R}} x^2 d\rho_j(x) \right)_{j \in [d]}$
- Variance: $F_{\text{var}} \stackrel{\text{def}}{=} (\text{Var}(\rho_j))_{j \in [d]}$
- Mean + Variance : $[F_{\text{mean}}(\rho), F_{\text{var}}(\rho)].$

Above, $\rho \in \mathcal{P}(\mathbb{R}^d)$, ρ_j is the j -th marginal of ρ , and $p \in \{d, 2d\}$ depends on the choice of the observable.

SMD General Recipe. The method consists in adding a stochastic perturbation in Eq. 2 according to the following equation:

$$dX_t^i = b(X_t^i, \hat{\rho}_{X_t}) dt + \sigma(X_t^i, \hat{\rho}_{X_t}) dB_t^i + \beta [\tilde{b}(X_t^i, \hat{\rho}_{X_t}) dt + \tilde{\sigma}(X_t^i, \hat{\rho}_{X_t}) dB_t]. \quad (4)$$

where $\beta \geq 0$ is an intensity parameter and B_t is a p -dimensional Brownian motion acting on all particles. The resulting dynamics Eq. 4 can thus be viewed as a combination of two effects: a deterministic mean-field drift—associated to b and σ (driving the system toward minimizers of the objective function), and a stochastic perturbation (associated to \tilde{b} and $\tilde{\sigma}$) providing macroscopic exploration. The intensity β of this additional exploration perturbation can be tuned in close analogy with the role of temperature in the finite-dimensional Langevin dynamics Eq. 1.

Consider independently the additional perturbation driven by \tilde{b} and $\tilde{\sigma}$:

$$dY_t^i = \tilde{b}(Y_t^i, \hat{\rho}_{Y_t}) dt + \tilde{\sigma}(Y_t^i, \hat{\rho}_{Y_t}) dB_t. \quad (5)$$

The coefficients \tilde{b} and $\tilde{\sigma}$ are defined so that the chosen macroscopic quantity of $\hat{\rho}_{Y_t}$, independently from the number N of particles in the system, solves the stochastic differential equation given by some coefficients $a \in \mathbb{R}^p$ and $s \in \mathbb{R}^{p \times p}$:

$$dF(\hat{\rho}_{Y_t}) = a(F(\hat{\rho}_{Y_t})) dt + s(F(\hat{\rho}_{Y_t})) dB_t. \quad (6)$$

The expression of \tilde{b} and $\tilde{\sigma}$ is given by an explicit formula from Germain & Monmarché (2025) and only depends on F , a and s . Therefore, given a choice of a macroscopic quantity F , a critical aspect of the method lies in the choice of the coefficients a and s . When F is positive, a, s are chosen such that Eq. 6 is a Bessel process in such way that $F(\hat{\rho}_{Y_t})$ stay positive, i.e.

$$a_+^\delta(z) = \left(\frac{\delta - 1/2}{z_i} \right)_{i \in [d]}, \quad s_+^\delta(z) = I_d$$

where $\delta \geq 2$ is a parameter whose role will be explained later. The formula of $(\tilde{b}, \tilde{\sigma})$ are given for any choice of perturbation $F \in \{F_{\text{mean}}, F_{\text{s.m.}}, F_{\text{var}}, [F_{\text{mean}}, F_{\text{var}}]\}$ in the following lemma.

Lemma 3.1. SMD-Mean $F = F_{\text{mean}}$, $(a, s) = (0_d, I_d)$.

$$\tilde{b}(x, \rho) \stackrel{\text{def}}{=} 0, \quad \tilde{\sigma}(x, \rho) \stackrel{\text{def}}{=} I_d, \quad (7)$$

SMD Second-order moment $F = F_{\text{s.m.}}$, $(a, s) = (a_+^\delta, s_+^\delta)$.

$$\begin{aligned} \tilde{b}(x, \rho) &\stackrel{\text{def}}{=} \left(\delta - \frac{3}{2} \right) \left[\frac{x}{4m_2(\rho)^2} \right], \\ \tilde{\sigma}(x, \rho) &\stackrel{\text{def}}{=} \text{Diag} \left[\frac{x}{2m_2(\rho)} \right]. \end{aligned} \quad (8)$$

SMD Variance $F = F_{\text{var}}$, $(a, s) = (a_+^\delta, s_+^\delta)$.

$$\begin{aligned} \tilde{b}(x, \rho) &\stackrel{\text{def}}{=} \left(\delta - \frac{3}{2} \right) \left[\frac{x - m(\rho)}{4 \text{Var}(\rho)^2} \right], \\ \tilde{\sigma}(x, \rho) &\stackrel{\text{def}}{=} \text{Diag} \left[\frac{x - m(\rho)}{2 \text{Var}(\rho)} \right]. \end{aligned} \quad (9)$$

SMD (Mean + variance) $F = [F_{\text{mean}}, F_{\text{var}}]$, $(a, s) = ((0_d, a_+^\delta), (I_d, s_+^\delta))$.

$$\tilde{\sigma}(x, \rho) \stackrel{\text{def}}{=} \left(I_d, \text{Diag} \left[\frac{x - m(\rho)}{2 \text{Var}(\rho)} \right] \right), \quad (10)$$

where $\tilde{b}(x, \rho)$ is the same of the variance perturbation case.

The derivation of the coefficients \tilde{b} and $\tilde{\sigma}$ is detailed in Appendix E.1, which were given only for dimension $d = 1$ in Germain & Monmarché (2025). The empirical efficiency of these methods is tested on a benchmark of multi-modal functions across multiple MKV dynamics in Section 4. Depending on the nature of the objective function to minimize, one should adapt its choice of perturbed macroscopic observable to maximize the efficiency of the method, even though Mean+Var will be recommended as a practical default.

Positivity constraints and Bessel dynamics. For a given macroscopic observable F , poorly chosen coefficients a and s may cause the dynamics Eq. 5 and Eq. 4 to blow up in finite time. This issue arises because many macroscopic observables (e.g., variances) take values in a restricted subset of \mathbb{R}^p . As long as the stochastic perturbation of $F(\hat{\rho}_{Y_t})$ remains within its admissible domain, the dynamics are well defined; however, if positivity constraints are violated, the coefficients become singular and the evolution breaks down.

To enforce positivity when perturbing second-order moments or variances, the coefficients a and s are chosen as d independent δ -Bessel processes (Revuz & Yor, 2013, Chapter 11), which preserve positivity for $\delta \geq 2$. These correspond to the SDE Eq. 6 with $(a, s) = (a_+^\delta, s_+^\delta)$, understood component-wise. In contrast, since the mean is unconstrained, its perturbation is taken to be standard Brownian motion ($a = 0, s = I_d$).

The coefficients defined in Eq. 8, Eq. 9, and Eq. 10, are not globally Lipschitz in ρ , reflecting potential singular behavior as second-order moments or variances approach zero. While this could in principle lead to finite-time explosion, Germain & Monmarché (2025, Section 6) show that the stochastic perturbation alone is non-explosive. It is therefore conjectured that the full dynamics Eq. 4, combining this perturbation with a broad class of mean-field optimization algorithms, is also non-explosive under mild conditions. Since no explosion was observed in our numerical experiments, we do not consider regularized dynamics in the remainder of this paper.

3.2. Noise using tangent space

The second approach relies on the geometric structure of the considered probability law space related to a dynamic. We introduce an infinite-dimensional noise that we claim to be canonical by injecting noise in tangent spaces related to the curve $t \mapsto \rho_t$. For the presentation of the approach, we follow the case-study of Stein variational gradient descent (SVGD). As Langevin, SVGD is a sampling method that can be used for global optimization (Serré et al., 2025). The recipe is summarized at the end of the section, the simulation scheme is detailed in Appendix B and all the proofs are given in Appendix E.

SVGD mean-field dynamics. Given a kernel $k : (x, y) \in \mathbb{R}^d \times \mathbb{R}^d \mapsto k(x, y)$, typically a Gaussian kernel $k = k_\sigma^{(d)}$, the SVGD’s N -particle dynamic is a MKV dynamics using b^{svgd} Eq. 3 as drift and with zero diffusion.

When $N \rightarrow \infty$, and under mild conditions, $\hat{\rho}_{X_t} \rightarrow \rho_t^{\text{svgd}}$ following the mean-field dynamics:

$$\partial_t \rho_t^{\text{svgd}} = -\text{div} \left(b^{\text{svgd}}(\cdot, \rho_t^{\text{svgd}}) \rho_t^{\text{svgd}} \right) \quad (11)$$

As Langevin dynamics, when $t \rightarrow \infty$, ρ_t^{svgd} is proved to converge to the Gibbs measure $\mu(x) \propto \exp(-V(x)/\kappa)$ related to potential V . In the following, we set the temperature parameter $\kappa = 1$.

In the following, we detail the structure of Eq. 11 to clarify the ρ -noise.

Gradient flow on Wasserstein space. Eq. 11 is in fact a gradient flow related to a specific geometry on the space of probability law (Duncan et al., 2023). To give an intuition on this interpretation, note that a sum of two probability measures (ρ, ν) is not a probability measure $\rho + \nu$ since $(\rho + \nu)(\mathbb{R}^d) = 2$. Instead, due to mass conservation, the following property holds: if a curve $t \in [0, 1] \rightarrow \rho_t \in \mathcal{P}_2 = \{\rho \in \mathcal{P}(\mathbb{R}^d) : \mathbb{E}_\rho [|X|^2] < \infty\}$ is absolutely continuous, then it satisfies the continuity equation in the sense of distribution (Ambrosio et al., 2005, Theorem 8.3.1), i.e. there

exists $v_t \in L^2(\rho_t)$ for any $t \in [0, 1]$ such that

$$\partial_t \rho_t + \text{div}(\rho_t v_t) = 0. \quad (12)$$

This means that an infinitesimal displacement around ρ_t has the form $\text{div}(\rho_t v_t)$.

Note that the discretization of Eq. 12 can be derived using:

$$\hat{\rho}_{(n+1)\varepsilon} = (id + \varepsilon v_{n\varepsilon}) \# \hat{\rho}_{n\varepsilon}, \quad (13)$$

$$\text{since} \quad \lim_{\varepsilon \rightarrow 0} \frac{(id + v_t) \# \rho_t - \rho_t}{\varepsilon} = \text{div}(\rho_t v_t). \quad (14)$$

For these reasons, the functional space where v_t belongs can be identified as a tangent space using Riemannian geometry vocabulary, and by using the pushforward operation ‘ $\#$ ’ instead of the addition ‘ $+$ ’. This statement is made rigorous in Ambrosio et al. (2005, Theorem 8.5.1).

In general, the tangent space is as subspace of:

$$L^2(\rho_t) = \left\{ f : \mathbb{R}^d \mapsto \mathbb{R}^d \text{ measurable} : \int \|f\|^2 d\rho_t < \infty \right\}.$$

In the case of SVGD dynamics, the functional space is related to a subspace of a Reproducible Kernel Hilbert Space (RKHS) $\mathcal{H}_d \subset L^2(\rho_t)$ generated by $K_{\text{SVGD}} = kI_d$ (Duncan et al., 2023).

Therefore, to *inject canonical noise* in a trajectory of probability laws (ρ_t) , we only have to inject canonical noise in the tangent space where v_t belongs according to its structure,

$$\hat{\rho}_{(n+1)\varepsilon} = (id + \varepsilon v_{n\varepsilon} + \sqrt{\varepsilon} G_n) \# \hat{\rho}_{n\varepsilon}, \quad G_n \sim \mathcal{G}. \quad (15)$$

The question is then, how to add canonical noise in the tangent space such that its time increments $(G_n)_{n \in \mathbb{N}} \sim \mathcal{G}$ act as an additive noise in equation Eq. 15? Can we characterize their law \mathcal{G} , as well as the law ρ^* of the resulting continuous time noising process?

Canonical noise in RKHS. Brownian motion, or any Gaussian process, is a random variable in an Hilbert space of functions typed as $\mathbb{R} \rightarrow \mathbb{R}$. Its natural generalization to Hilbert spaces of functions $\mathbb{R}^d \rightarrow \mathbb{R}^d$ is called a d -dimensional space Gaussian process, or Gaussian random field (Estrade & Fournier, 2025; MacKay et al., 1998). In the following, we focus on RKHS-valued Gaussian random fields.

Definition 3.2 (\mathcal{H}_d -Gaussian random field). A random variable $G : \Omega \rightarrow \mathcal{H}_d$ is called a (centered) \mathcal{H}_d -Gaussian random field if, for every $f \in \mathcal{H}_d$, the real-valued random variable $\langle G, f \rangle_{\mathcal{H}_d}$ is a centered Gaussian random variable on \mathbb{R} . Moreover, if $\mathbb{E} \|G\|_{\mathcal{H}_d}^2 < \infty$, then its law is characterized by a covariance kernel $K : \mathbb{R}^d \times \mathbb{R}^d \mapsto \mathcal{S}_d^{++} \subset \mathbb{R}^{d \times d}$ and we denote $G \sim \mathcal{G}(K)$. More precisely, for any $X = (x_i)_{i \in [N]} \in (\mathbb{R}^d)^N$, $(G(x_i))_{i \in [N]}$ is a \mathbb{R}^{Nd} Gaussian vector, whose covariance matrix $K(X) = (K_{i,j}(X))_{i,j \in [N]} \in \mathbb{R}^{Nd \times Nd}$ is given by the blocs:

$$K_{i,j}(X) = K(x_i, x_j) = \mathbb{E}[G(x_i)G(x_j)^T] \in \mathbb{R}^{d \times d}. \quad (16)$$

Heuristically, a centered Gaussian process G with covariance kernel \bar{K} can be interpreted as a standard Gaussian on the RKHS \mathcal{H}_d , formally associated with density $\exp(-\frac{1}{2}\|G\|_{\mathcal{H}_d}^2)$. This interpretation cannot be made rigorous in \mathcal{H}_d , since infinite-dimensional Hilbert spaces do not admit a Lebesgue reference measure. A rigorous meaning is obtained by restricting G to finite-dimensional subspaces \mathcal{H}_d^X generated by kernel evaluations:

$$\mathcal{H}_d^X = \text{span}(K(x_i, \cdot)e_j, i, j \in [N] \times [d]) \subset \mathcal{H}_d.$$

by considering its orthogonal projection $\pi_X G$ into \mathcal{H}_d^X .

Lemma 3.3. *Let $X = (x_1, \dots, x_N)$ with $x_i \neq x_j$ if $i \neq j$, and let $G \sim \mathcal{G}(K_{\text{SVGD}})$. Then the projection $\pi_X G \in \mathcal{H}_d^X$ admits a density $\mathbb{P}(\pi_X G \in df)$ with respect to the Lebesgue measure induced by the RKHS inner product, given by*

$$\mathbb{P}(\pi_X G \in df) \propto \exp(-\frac{1}{2}\|f\|_{\mathcal{H}_d}^2).$$

Equivalently, $G(X) = (G(x_1), \dots, G(x_N)) \in \mathbb{R}^{Nd}$ is a centered Gaussian vector with density proportional to $\exp(-\frac{1}{2}g^\top \bar{K}(X)^{-1}g)$ with respect to the usual Lebesgue measure on \mathbb{R}^{Nd} .

All theoretical details are deferred to Appendix E.2.

Lemma 3.3 justifies that $G \sim \mathcal{G}(K_{\text{SVGD}})$ is Gaussian standard in \mathcal{H}_d , and thus is considered canonical.

The following remark justifies that d -dimensional space Gaussian process is an infinite dimensional noise.

Remark 3.4. When the kernel $k(x, y) = k_\sigma^{(d)}(x, y)$ is Gaussian, $G \stackrel{\text{def}}{=} (G_i)_{i \in [d]} \sim \mathcal{G}(K_{\text{SVGD}})$ can be simulated as follows (Lototsky et al., 2017, Eq (1.1.11))

$$G_i = \sum_{\vec{n} \in \mathbb{N}^d} \lambda_{\vec{n}} \varphi_{\vec{n}}(\cdot) \xi_{\vec{n}}^i, \quad \xi_{\vec{n}}^i \stackrel{i.i.d.}{\sim} \mathcal{N}(0, 1), \quad \vec{n} \in \mathbb{N}^d$$

where $(\Phi_{\vec{n}} = \sqrt{\lambda_{\vec{n}}} \varphi_{\vec{n}})_{\vec{n} \in \mathbb{N}^d}$ is an orthonormal basis of the RKHS related to $k_\sigma^{(d)}$ (Berlinet & Thomas-Agnan, 2011).

The take-home message is the following : if we aim to inject canonical noise in the SVGD, we should add time-dependent noise in Eq. 12, whose time increments are i.i.d \mathcal{H}_d -Gaussian random field of covariance kernel K_{SVGD} , i.e. $\mathcal{G} = \mathcal{G}(\beta^2 K_{\text{SVGD}})$ in Eq. 15 where $\beta > 0$ is a temperature parameter.

Continuous Langevin-type dynamics. Our goal is to study the time-continuous dynamics related to in Eq. 15 when injecting canonical noise $\mathcal{G} = \mathcal{G}(\beta^2 K_{\text{SVGD}})$, to get a Langevin-type dynamic on the space of probability laws, corresponding to a gradient flow Eq. 12 with a canonical ρ -noise. Since the continuity equation is a partial differential equation, its stochastic counterpart naturally takes the

form of a stochastic partial differential equation (SPDE). Accordingly, the noise must be modeled as a Gaussian space-time process $(G_t)_{t \geq 0} \sim \mathcal{T}\mathcal{G}(K_{\text{SVGD}})$ with increments $G_{t+\varepsilon} - G_t \sim \mathcal{G}(\varepsilon K_{\text{SVGD}})$, which can be viewed as the infinite-dimensional analogue of Brownian motion. In the SPDE, this leads to the appearance of the infinitesimal noise term dG_t , interpreted as Gaussian white noise, that is, the distributional time derivative of G_t (Lototsky et al., 2017, Eq. (1.1.5)); see Appendix D for an introduction to these objects.

Following Remark 3.4, in the case of SVGD, the infinitesimal variation of $(G_t)_{t \geq 0} = (G_t^i)_{i \in [d], t \geq 0} \sim \mathcal{T}\mathcal{G}(K_{\text{SVGD}})$ can be represented as follows,

$$dG_i(t, \cdot) = \sum_{\vec{n} \in \mathbb{N}^d} \lambda_{\vec{n}} \varphi_{\vec{n}}(\cdot) d\xi_{\vec{n}, t}^i, \quad (17)$$

where $(\xi_{\vec{n}, t}^i)_{t \geq 0}$ are independent Brownian motions (Lototsky et al., 2017, Eq (1.1.10)).

To define a valid SPDE, the idea is first to consider the simplified case where $\rho_0 = \hat{\rho}_0$ is the empirical measure of a particle system. Because the dynamic of the system is fully described by the motion of the N particles, the SPDE can be rewritten as an SDE governing the evolution the particles. The initial SPDE is then obtained as a limit of the considered SDEs as $N \rightarrow \infty$. The SDE describing the motions of N particles is derived from equation

Lemma 3.5. *The SDE being the time-continuous/discretized in space version of Eq. 15 with $\mathcal{G} = \mathcal{G}(\beta^2 K_{\text{SVGD}})$ and $\beta > 0$ is*

$$d\bar{X}_t = b^{\text{svgd}}(X_t, \rho_t^N) dt + \beta \bar{K}^{1/2}(X_t) dB_t^{Nd}, \quad (18)$$

with $\rho_t^N = \frac{1}{N} \sum_{i=1}^N \delta_{X_t^i}$ is the empirical measure of the particle system, $(B_t^{Nd})_{t \geq 0}$ is a Nd dimensional Brownian motion and $\bar{K}(X) = K(X) \otimes I_d \in \mathbb{R}^{dN \times dN}$, $K(X) \stackrel{\text{def}}{=} (k(X^i, X^j))_{i, j \in [N]}$.

In the following, the term:

$$\bar{K}(X_t)^{1/2} dB_t^{Nd} \quad (19)$$

will be referred as *Geometrical Common Noise* (GCN). This diffusion coefficient is the consequence of the addition of the $\sqrt{\varepsilon}G_n$ term in Eq. 15.

Surprisingly, when $\beta = \beta_N \stackrel{\text{def}}{=} \sqrt{2}/\sqrt{N}$ the dynamic Eq. 18 was already studied in the literature under the name of Stochastic Langevin with repulsive force; see (Gallego & Insua, 2018; Nüsken & Renger, 2021) and (Duncan et al., 2023, Section 3). In this setting the noise vanishes at the large N limit and the evolution of ρ_t^N becomes deterministic. In this paper, under the scaling $\beta_N = \beta > 0$, the noise Eq. 19 doesn't vanish when $N \rightarrow \infty$, thus GCN is a ρ -noise.

In the following theorem $t \rightarrow \rho_t^*$ is the noised dynamic $t \rightarrow \rho_t^{\text{svgd noisy}}$ that we look for.

Theorem 3.6. *If the family $\{\rho_t^N : N \in \mathbb{N}\}$ possesses a limit point in $\mathcal{P}(C[0, T])$ denoted by ρ^* , then ρ^* is solution in the weak sense of*

$$\begin{aligned} \partial_t \rho_t^* + \text{div}((b(\cdot, \rho_t^*) + \beta dG_t)) \rho_t^* \\ + \beta^2 \Delta_t(k(\cdot, \cdot) \rho_t^*) = 0, \quad G \sim \mathcal{TG}(K_{\text{SVGD}}) \end{aligned} \quad (20)$$

Moreover, in case where $k(x, x) = 1$ for any $x \in \mathbb{R}^d$, which is verified when $K_{\text{SVGD}} = k_\sigma^{(d)} I_d$, ρ_t^* can be approximated using that

$$\begin{cases} \rho_{t+\varepsilon}^* \approx (id + T_t) \# \rho_t^*, \quad g_t \sim \mathcal{G}(K_{\text{SVGD}}) \\ T_t = \varepsilon b(\cdot, \rho_t^*) + \sqrt{\varepsilon} \beta g_t. \end{cases} \quad (21)$$

In practice, only the dynamics of N particles is simulated using Eq. 18, whose the Euler-Maruyama integration scheme is given with details in Appendix B. In our experiments the kernel k is Gaussian. The scheme given in Eq. 21 is here only to give more intuition on dG in Eq. 20, which becomes βg_t in Eq. 21, accounting the stochastic limit-effect of the infinitesimal d -dimensional space Gaussian process noise that was injected in Eq. 18.

By seeing $t \rightarrow \rho_t^{\text{svgd}}$ as a gradient flow on a Wasserstein space (Duncan et al., 2023), the dynamic $t \rightarrow \rho_t^*$ given in Theorem 3.6 can be seen as a Langevin dynamic on the space of probability law related to the metric given in Duncan et al. (2023, Definition 7), that is why we consider the noise Eq. 19 as canonical compared to SMD (Section 3.1).

Generalization of the approach. In general, the kernel related to SVGD and the Gaussian process covariance function could be chosen differently, and the noise given by Eq. 19 can be added to any MKV dynamics, the limit-effect will keep the same structure than for SVGD. However, GCN cannot be considered as canonical if there is no link to the gradient flow structure of the original dynamic.

In any case, the choice of the kernel should encode the regularity prior on the objective function. In experiments, the effect of the bandwidth σ is studied when the covariance function is Gaussian ($k_\sigma I_d$).

Link between GCN and SMD-mean. The following Theorem shows that GCN is an interpolation between an infinite-dimensional white noise and SMD-mean, which is a d -dimensional noise, depending on the bandwidth parameter σ when $k = k_\sigma^{(d)}$.

Theorem 3.7. *If the covariance function $k_\sigma^{(d)}$ is Gaussian:*

- If the parameter $\sigma \rightarrow \infty$, GCN is SMD-mean.
- If the parameter $\sigma \rightarrow 0$, GCN is a white noise.

4. Numerical Experiments

We validate our noise injection methods on multimodal benchmark functions (Serré et al., 2025; Pinna et al., 2017; Malherbe & Vayatis, 2017), comparing standard MKV dynamics (CBO, SBS, Langevin, MSGD) against their SMD and GCN variants. Implementation uses C++ with Eigen and Python bindings¹, with Euler-Maruyama schemes from Appendices A and B.

Computational Complexity. SMD incurs $\mathcal{O}(N)$ complexity per iteration ($\mathcal{O}(1)$ for mean perturbation), while GCN requires $\mathcal{O}(N^3)$ for covariance matrix square root computation, making SMD significantly more efficient for large particle systems.

Each dynamic is evaluated on 7 multimodal benchmarks in dimension 20 with 150 particles over 300 iterations, averaged over 50 runs. Parameters: stepsize $dt = 0.1$, SBS kernel bandwidth $1/N^2$ (Serré et al., 2025), CBO parameters $\lambda = 1, \varepsilon = 10^{-2}, \beta = 1, \sigma = 5.1$ (Carrillo et al., 2021), Langevin temperature $\beta = 1$, GCN Gaussian kernel bandwidth $\sigma = 1$. To assess statistical significance, we perform one or several Mann-Whitney U tests depending on which type of method achieves the best result: if a vanilla dynamic achieves the best result, we compare it against all its SMD and GCN variants; if a SMD or GCN variant achieves the best result, we compare it only against the vanilla dynamic.

Best results are in **bold**. Mann-Whitney U tests at level 0.05 are highlighted in **gray**. We report average rank and empirical competitive ratio (ECR), $\text{ECR}(m) = \frac{1}{|F|} \sum_{f \in F} \min(100, df_m / df^*)$, where df_m is the distance to optimum for method m and df^* is the best distance.

Table 1 shows that noise injection consistently enhances baseline performance. SMD variants generally outperform GCN, with significant gains for CBO. MSGD, Langevin and SBS also benefit from noise injection, showing reliable improvements across multiple benchmarks. Figure 1 shows SMD mean perturbation improves CBO and MSGD on Ackley ($d = 4$). Figure 2 demonstrates GCN’s robustness to kernel bandwidth σ on Levy ($d = 10$).

Problem-Dependent Effects. More broadly, Table 1 and Figures 1 and 2 reveal that noise injection effectiveness is intimately tied to both the baseline dynamic and problem characteristics. A critical factor is the particle-to-dimension ratio. When the number of particles is sufficiently large relative to the problem dimension, the baseline dynamics converge reliably, and the added noise provides no substantial benefit (see Figure 3a). In fact, it may even degrade performance by introducing unnecessary perturbations. Conversely, when particles are scarce relative to dimension, the additional exploration provided by noise injection yields

¹Anonymous link upon acceptance

Table 1. Comparison between vanilla dynamics and their SMD and GCN variants on 7 multimodal benchmark functions in dimension 20 using 150 particles over 300 iterations. For each dynamic, the average best result is reported. The average rank over all benchmarks along with the ECR is reported at the bottom of each table. The maximum p-value of Mann-Whitney U tests is reported in the last column. The best results are in bold and cells where the Mann-Whitney U test is significant at level 0.05 are highlighted in gray.

	Benchmark	CBO	SMD-CBO Mean	SMD-CBO M ²	SMD-CBO Var	SMD-CBO Mean+Var	GCN-CBO	p-value
CBO dynamics	Ackley	21.097	20.615	21.083	21.088	20.610	20.591	0.000
	Deb N.1	-1.000	-1.000	-1.000	-1.000	-1.000	-1.000	0.000
	Griewank	20.279	19.562	19.657	19.683	20.073	19.506	0.237
	Levy	102.351	86.857	95.816	95.945	81.912	85.146	0.000
	Rastrigin	253.358	238.943	250.021	250.463	240.406	238.768	0.000
	Schwefel	5157.189	5127.111	5139.564	5146.530	5199.557	5111.855	0.387
	Styblinski-Tang	-19.513	-20.798	-20.006	-19.881	-20.091	-20.191	0.000
	Avg Rank	5.14	2.00	3.29	4.14	3.00	1.29	
SBS dynamics	ECR	1.0648	1.0097	1.0424	1.0443	1.0132	1.0104	
	Benchmark	SBS	SMD-SBS Mean	SMD-SBS M ²	SMD-SBS Var	SMD-SBS Mean+Var	GCN-SBS	p-value
Ackley	21.126	20.851	21.112	21.102	20.825	20.810	0.000	
Deb N.1	-0.961	-0.835	-1.000	-1.000	-1.000	-0.909	0.000	
Griewank	19.959	19.686	20.646	20.218	19.953	19.128	0.173	
Levy	24.036	47.680	25.827	25.815	46.601	45.794	0.005	
Rastrigin	86.442	185.464	83.496	80.785	190.917	181.370	0.006	
Schwefel	5986.360	5984.992	5989.562	6062.542	5947.981	5985.055	0.365	
Langevin dynamics	Styblinski-Tang	-25.668	-24.339	-23.746	-24.191	-24.578	-25.150	0.008
	Avg Rank	3.29	4.00	4.29	3.57	3.00	2.86	
	ECR	15.1622	15.4879	15.1930	15.1820	1.3467	15.4564	
	Benchmark	Langevin	SMD-Langevin Mean	SMD-Langevin M ²	SMD-Langevin Var	SMD-Langevin Mean+Var	GCN-Langevin	p-value
Ackley	20.723	20.767	20.732	20.733	20.757	20.760	1.000	
Deb N.1	-0.921	-0.956	-1.000	-1.000	-1.000	-0.958	0.000	
Griewank	19.362	19.117	18.711	19.193	18.992	18.516	0.097	
Levy	1.329	1.847	1.173	1.073	1.904	1.796	0.000	
MSGD dynamics	Rastrigin	184.367	189.482	183.202	184.258	193.141	187.751	0.677
	Schwefel	2405.830	2436.136	2383.227	2324.940	2381.518	2404.611	0.316
	Styblinski-Tang	-34.902	-33.186	-35.050	-34.914	-32.868	-33.206	0.278
	Avg Rank	3.86	5.14	2.00	2.14	4.00	3.71	
	ECR	15.1944	15.3272	15.1613	1.0108	1.2014	15.3117	
	Benchmark	MSGD	SMD-MSGD Mean	SMD-MSGD M ²	SMD-MSGD Var	SMD-MSGD Mean+Var	GCN-MSGD	p-value
Ackley	19.977	20.725	19.985	19.982	20.736	20.736	0.497	
Deb N.1	-0.567	-0.834	-1.000	-1.000	-1.000	-0.920	0.000	
Griewank	19.467	18.829	19.557	20.007	19.254	19.358	0.243	
Levy	9.413	1.905	8.873	9.330	1.888	1.354	0.000	
Langevin dynamics	Rastrigin	187.689	187.206	193.505	186.581	183.479	183.768	0.278
	Schwefel	2396.030	2424.021	2361.875	2386.382	2380.197	2447.570	0.488
	Styblinski-Tang	-36.325	-34.665	-36.379	-36.353	-34.457	-34.867	0.042
	Avg Rank	4.14	3.86	3.00	3.14	2.86	3.57	
	ECR	16.0058	15.3008	1.8064	1.8554	1.1646	15.2352	

modest but consistent improvements by helping particles escape local minima (see Figure 3b). These findings suggest that reproducing our results in higher dimensions requires careful tuning of particle counts to maintain the balance observed in our $d = 20$ experiments. Specifically, one should increase the number of particles proportionally to avoid regime shifts where noise becomes detrimental. Developing adaptive strategies for automatically selecting noise injection methods and hyperparameters based on the problem’s intrinsic dimensionality remains an important direction for future work.

Unimodal Functions. We evaluate noise injection on a set of unimodal benchmark functions in dimension 20 with 150 particles over 300 iterations. The results (detailed in Table 2) reveal similar trends as in the multimodal case for CBO dynamics, but more mixed outcomes for gradient-aware methods. This aligns with the intuition that noise injection primarily aids exploration in multimodal landscapes. For convex functions with a single global minimum, the

added stochasticity provides limited advantage to methods that already leverage gradient information effectively, and may even degrade performance by introducing unnecessary perturbations (see Figure 4).

5. Conclusion

This work addresses a key limitation of MKV optimization methods: deterministic mean-field dynamics that hinder exploration. Viewing MKV systems as a unifying framework for methods such as CBO and SBS, we proposed two principled ways to inject common noise: a perturbative approach based on conditional MKV theory and a geometric approach exploiting tangent-space structure. Treating noise as a modular component makes our framework applicable to *any* MKV algorithm. Experiments show that both strategies improve exploration and convergence. We recommend **SMD Mean+Var** as a practical default, combining strong empirical performance with $\mathcal{O}(N)$ computational cost, compared to $\mathcal{O}(N^3)$ for GCN. Future work will focus

on adaptive parameter tuning and extensions beyond global optimization.

Acknowledgments

G.S., S.G., and A.K. acknowledge support from the Industrial Data Analytics and Machine Learning Chair hosted at ENS Paris-Saclay, Université Paris-Saclay.

Impact Statement

This paper presents work whose goal is to advance the field of Optimization. There are many potential societal consequences of our work, none which we feel must be specifically highlighted here.

References

Ambrosio, L., Gigli, N., and Savaré, G. *Gradient flows: in metric spaces and in the space of probability measures*. Springer, 2005.

Awasthi, P., Mao, A., Mohri, M., and Zhong, Y. DC-programming for neural network optimizations. *Journal of Global Optimization*, 2024.

Berlinet, A. and Thomas-Agnan, C. *Reproducing kernel Hilbert spaces in probability and statistics*. Springer, 2011.

Carmona, R. and Delarue, F. *Probabilistic Theory of Mean Field Games with Applications*, volume II. Springer, 2018.

Carmona, R., Delarue, F., et al. *Probabilistic theory of mean field games with applications I-II*, volume 3. Springer, 2018.

Carrillo, J. A., Jin, S., Li, L., and Zhu, Y. A Consensus-Based Global Optimization Method for High Dimensional Machine Learning Problems. *ESAIM: Control, Optimisation and Calculus of Variations*, 27:S5, 2021.

Da Prato, G. and Zabczyk, J. *Stochastic equations in infinite dimensions*, volume 152. Cambridge University Press, 2014.

Delarue, F. and Hammersley, W. R. Rearranged stochastic heat equation. *Probability Theory and Related Fields*, 191(1):41–102, 2025.

Delarue, F. and Vasileiadis, A. Exploration noise for learning linear-quadratic mean field games. *Mathematics of Operations Research*, 50(3):1762–1831, 2025.

Delarue, F., Tanré, E., and Maillet, R. Ergodicity of some stochastic Fokker-Planck equations with additive common noise. *Preprint arXiv:2405.09950*, 2024.

Duncan, A., Nüsken, N., and Szpruch, L. On the geometry of Stein variational gradient descent. *Journal of Machine Learning Research*, 24(56):1–39, 2023.

El Yadari, M., El Motaki, S., Yahyaouy, A., Makany, P., El Fazazy, K., Gualous, H., and Le Masson, S. Taxonomy of optimization algorithms combined with CNN for optimal placement of virtual machines within physical machines in data centers. *Energy Informatics*, 2024.

Estrade, A. and Fournier, J. Gaussian Fields Through Geometrical Properties. In *Stochastic Geometry: Percolation, Tesselations, Gaussian Fields and Point Processes*, pp. 81–131. Springer, 2025.

Fornasier, M., Klock, T., and Riedl, K. Consensus-based optimization methods converge globally. *SIAM Journal on Optimization*, 34(3):2973–3004, 2024.

Franceschi, L., Donini, M., Perrone, V., Klein, A., Archambault, C., Seeger, M., Pontil, M., and Frasconi, P. Hyperparameter optimization in machine learning. *Preprint arXiv:2410.22854*, 2024.

Gallego, V. and Insua, D. R. Stochastic gradient MCMC with repulsive forces. *Preprint arXiv:1812.00071*, 2018.

Germain, P. and Monmarché, P. Stochastic moments dynamics: a flexible finite-dimensional random perturbation of Wasserstein gradient descent. *Preprint arXiv:2505.07448*, 2025.

Houssein, E. H., Saeed, M. K., Hu, G., and Al-Sayed, M. M. Metaheuristics for Solving Global and Engineering Optimization Problems: Review, Applications, Open Issues and Challenges. *Archives of Computational Methods in Engineering*, 2024.

Hwang, C.-R. Laplace’s method revisited: weak convergence of probability measures. *The Annals of Probability*, pp. 1177–1182, 1980.

Karatzas, I. and Shreve, S. *Brownian motion and stochastic calculus*, volume 113. Springer, 1991.

Kirkpatrick, S., Gelatt, C. D., and Vecchi, M. P. Optimization by simulated annealing. *Science*, 220(4598):671–680, 1983.

Koß, M., Weissmann, S., and Zech, J. On the mean field limit of consensus based methods. *Preprint arXiv:2409.03518*, 2024.

Lee, J., Lee, I.-H., Joung, I., Lee, J., and Brooks, B. R. Finding multiple reaction pathways via global optimization of action. *Nature Communications*, 2017.

Lototsky, S. V., Rozovsky, B. L., et al. *Stochastic partial differential equations*, volume 11. Springer, 2017.

MacKay, D. J. et al. Introduction to Gaussian processes.
NATO ASI series F Computer and Systems Sciences, 168: 133–166, 1998.

Maillet, R. A Note on the Long-Time Behaviour of Stochastic McKean–Vlasov Equations with Common Noise.
Preprint arXiv:2306.16130, 2023.

Malherbe, C. and Vayatis, N. Global optimization of Lipschitz functions. In *International Conference on Machine Learning*, 2017.

Monmarché, P. and Reygner, J. Local convergence rates for Wasserstein gradient flows and McKean–Vlasov equations with multiple stationary solutions. *Probability Theory and Related Fields*, pp. 1–59, 2025.

Nüsken, N. and Renger, D. Stein variational gradient descent: many-particle and long-time asymptotics. *Preprint arXiv:2102.12956*, 2021.

Øksendal, B. *Stochastic differential equations: an introduction with applications*. Springer Science & Business Media, 6th edition, 2013.

Pavliotis, G. A. *Stochastic processes and applications: diffusion processes, the Fokker-Planck and Langevin equations*, volume 60. Springer, 2014.

Pinna, R., Totzeck, C., Tse, O., and Martin, S. A Consensus-Based Model for Global Optimization and Its Mean-Field Limit. *Mathematical Models and Methods in Applied Sciences*, 27(1):183–204, 2017.

Pintér, J. D. Global Optimization in Action. *Nonconvex Optimization and Its Applications*, 1996.

Revuz, D. and Yor, M. *Continuous martingales and Brownian motion*, volume 293. Springer, 2013.

Roberts, G. O. and Tweedie, R. L. Exponential Convergence of Langevin Distributions and Their Discrete Approximations. *Bernoulli*, 2(4):341–363, 1996.

Serré, G., Kalogeratos, A., and Vayatis, N. Stein Boltzmann Sampling: A Variational Approach for Global Optimization. In *International Conference on Artificial Intelligence and Statistics*, 2025.

Sznitman, A.-S. *Topics in propagation of chaos*. Springer, 1991.

Tugaut, J. Phase Transitions of McKean–Vlasov Processes in Double-Well Landscape. *Stochastics*, 86(2):257–284, 2014.

A. Simulation scheme for Stochastic Moment Dynamics

We use an Euler-Maruyama discretization of equation Eq. 4 to compute the evolution of the particle system. Let $(\Delta t_n)_{n \in \mathbb{N}}$ be a sequence of positive (and possibly decreasing) time step and define the discrete times $t_n = \sum_{k=0}^n \Delta t_k$. The Euler-Maruyama scheme associated with Eq. 4 is given, for each particle $i \in [N]$, by

$$\begin{aligned} X_{n+1}^i &= X_n^i + \Delta t_{n+1} \cdot \left[b\left(X_n^i, \hat{\rho}_{X_n}\right) + \tilde{b}\left(X_n^i, \hat{\rho}_{X_n}\right) \right] \\ &\quad + \sqrt{\Delta t_{n+1}} \cdot \left[\sigma\left(X_n^i, \hat{\rho}_{X_n}\right) \xi_n^i + \tilde{\sigma}\left(X_n^i, \hat{\rho}_{X_n}\right) \zeta_n \right], \end{aligned} \quad (22)$$

where $(\xi_n^i)_{i \in [N], n \geq 0}$ and $(\zeta_n)_{n \geq 0}$ are independent standard Gaussian increments of respective dimension d and p .

B. Simulation scheme for Geometric Common Noise

We use an Euler-Maruyama discretization of equation Eq. 18 to compute the evolution of the particle system. Let $(\Delta t_n)_{n \in \mathbb{N}}$ be a sequence of positive (and possibly decreasing) time steps and define the discrete times $t_n = \sum_{k=0}^n \Delta t_k$. Denoting by k_{noise} the kernel used for Geometric Common Noise and k the kernel used for SVGD (in the presentation $k = k_{\text{noise}}$ to have a canonical meaning, but this is not necessary in general), the Euler-Maruyama scheme for the GCN-noised SVGD N -particle dynamics is given by:

$$\bar{X}_{n+1} = \bar{X}_n + \Delta t_{n+1} \cdot \bar{b}_n + \sqrt{\Delta t_{n+1}} \cdot \bar{K}_{\bar{X}_n}^{1/2} \bar{\xi}_n, \quad (23)$$

where $\bar{X}_n = (X_n^1, \dots, X_n^N) \in \mathbb{R}^{Nd}$ is the concatenated state of all particles at time t_n , and

$$\begin{aligned} \bar{b}_n &= (b^{\text{svgd}}(X_n^i, \hat{\rho}_{X_n}))_{i \in [N]}, \quad \hat{\rho}_{X_n} = \frac{1}{N} \sum_{i=1}^N \delta_{X_n^i}, \\ b^{\text{svgd}}(\cdot, \rho) &\triangleq \mathbb{E}_{X \sim \rho} \left[-k(\cdot, X) \nabla V(X) + \nabla_x k(\cdot, X) \right], \\ \bar{K}_{\bar{X}_n} &= K_{\bar{X}_n} \otimes I_d, \quad K_{\bar{X}_n} = (k_{\text{noise}}(X_n^i, X_n^j))_{(i,j) \in [N]^2} \in \mathbb{R}^{N \times N}, \\ \bar{\xi}_n &\sim \mathcal{N}(0_{Nd}, I_{Nd}) \text{ are independent standard Gaussian increments.} \end{aligned}$$

For other particle dynamics, GCN noise can also be incorporated by adding the term $\sqrt{\Delta t_{n+1}} \cdot \bar{K}_{\bar{X}_n}^{1/2} \bar{\xi}_n$ to the update scheme.

C. Background: Stochastic Differential Equations and McKean-Vlasov Theory

This appendix provides a self-contained introduction to stochastic differential equations (SDEs) and MKV dynamics, establishing the theoretical foundations underlying the methods presented in this paper.

C.1. Stochastic Differential Equations

A stochastic differential equation (SDE) describes the evolution of a random process by combining deterministic drift with random fluctuations (Øksendal, 2013; Karatzas & Shreve, 1991). The canonical form of an SDE in \mathbb{R}^d is:

$$dX_t = b(t, X_t)dt + \sigma(t, X_t)dB_t,$$

where $X_t \in \mathbb{R}^d$ is the state at time t , $b : [0, \infty) \times \mathbb{R}^d \rightarrow \mathbb{R}^d$ is the drift coefficient, $\sigma : [0, \infty) \times \mathbb{R}^d \rightarrow \mathbb{R}^{d \times m}$ is the diffusion coefficient, and $(B_t)_{t \geq 0}$ is an m -dimensional standard Brownian motion. The solution X_t is a continuous-time stochastic process whose law evolves according to the Fokker-Planck equation:

$$\partial_t \rho_t = -\nabla \cdot (b(t, \cdot) \rho_t) + \frac{1}{2} \sum_{i,j} \partial_{x_i x_j}^2 (a_{ij}(t, \cdot) \rho_t),$$

where ρ_t denotes the probability density of X_t and $a = \sigma \sigma^T$ is the diffusion matrix (Pavliotis, 2014).

Langevin dynamics. A fundamental example is the overdamped Langevin equation Eq. 1, which arises naturally in statistical mechanics and Bayesian sampling (Pavliotis, 2014). For a potential function $V : \mathbb{R}^d \rightarrow \mathbb{R}$ and temperature parameter $\varepsilon > 0$:

$$dX_t = -\nabla V(X_t)dt + \sqrt{2\varepsilon}dB_t.$$

Under suitable regularity conditions on V (e.g., smoothness and growth conditions), the law ρ_t of X_t converges as $t \rightarrow \infty$ to the Gibbs measure:

$$\rho_\varepsilon(dx) \propto \exp\left(-\frac{V(x)}{\varepsilon}\right)dx.$$

This convergence can be characterized through the evolution of the relative entropy (KL divergence) $\text{KL}(\rho_t \parallel \rho_\varepsilon)$, which decreases monotonically along trajectories. The Gibbs measure concentrates near the global minima of V as $\varepsilon \rightarrow 0$, making Langevin dynamics a natural tool for global optimization when combined with appropriate temperature scheduling (simulated annealing) (Kirkpatrick et al., 1983).

C.2. McKean-Vlasov Equations and Mean-Field Limits

MKV equations extend classical SDEs by allowing the drift and diffusion coefficients to depend on the probability distribution of the solution itself, creating a nonlinear feedback mechanism (Sznitman, 1991; Carmona et al., 2018). A MKV SDE takes the form:

$$dX_t = b(X_t, \rho_t)dt + \sigma(X_t, \rho_t)dB_t,$$

where ρ_t denotes the law of X_t at time t , and the coefficients $b : \mathbb{R}^d \times \mathcal{P}(\mathbb{R}^d) \rightarrow \mathbb{R}^d$ and $\sigma : \mathbb{R}^d \times \mathcal{P}(\mathbb{R}^d) \rightarrow \mathbb{R}^{d \times m}$ now depend on the entire probability measure $\rho \in \mathcal{P}(\mathbb{R}^d)$.

Particle approximation and propagation of chaos. In practice, MKV dynamics are approximated through interacting particle systems. Consider N particles (X_t^1, \dots, X_t^N) evolving according to:

$$dX_t^i = b(X_t^i, \hat{\rho}_{X_t})dt + \sigma(X_t^i, \hat{\rho}_{X_t})dB_t^i, \quad i = 1, \dots, N,$$

where $\hat{\rho}_{X_t} = \frac{1}{N} \sum_{i=1}^N \delta_{X_t^i}$ is the empirical measure of the particle system, and $(B_t^i)_{i=1}^N$ are independent Brownian motions. Under suitable Lipschitz conditions on the coefficients, the empirical measure $\hat{\rho}_{X_t}$ converges as $N \rightarrow \infty$ to the deterministic measure ρ_t satisfying the MKV equation. This phenomenon, known as *propagation of chaos* (Sznitman, 1991), ensures that particles become asymptotically independent and identically distributed according to ρ_t .

The mean-field limit reduces the stochastic particle system to a deterministic evolution on probability space governed by:

$$\partial_t \rho_t = -\nabla \cdot (b(\cdot, \rho_t)\rho_t) + \frac{1}{2} \sum_{i,j} \partial_{x_i x_j}^2 (a_{ij}(\cdot, \rho_t)\rho_t),$$

where $a(\cdot, \rho) = \sigma(\cdot, \rho)\sigma(\cdot, \rho)^T$. This is a nonlinear partial differential equation in the space of probability measures (Carmona et al., 2018).

Common Noise in MKV Systems. In standard MKV systems, the independent Brownian motions $(B_t^i)_{i=1}^N$ average out in the mean-field limit, making the evolution of ρ_t deterministic. To maintain stochasticity at the population level, one can introduce *common noise*, a Brownian motion W_t shared by all particles (Germain & Monmarché, 2025):

$$dX_t^i = b(X_t^i, \hat{\rho}_{X_t})dt + \sigma(X_t^i, \hat{\rho}_{X_t})dB_t^i + \tilde{\sigma}(X_t^i, \hat{\rho}_{X_t})dW_t.$$

Unlike the independent noise σdB_t^i which vanishes as $N \rightarrow \infty$, the common noise $\tilde{\sigma}dW_t$ persists in the mean-field limit, inducing a stochastic evolution of ρ_t . This enables collective transitions between basins of attraction, enhancing exploration in multimodal landscapes.

D. Background: Random Generalized Functions

Many stochastic models arising in machine learning, physics, and spatial statistics involve random objects that are too irregular to be defined pointwise. A convenient and rigorous framework to handle such objects is that of *random generalized functions* (also called distribution-valued random variables).

Let \mathcal{D} denote a space of test functions (e.g., $C_c^\infty(\mathbb{R}^d)$ or the Schwartz space \mathcal{S}). A generalized function is a continuous linear functional $T : \mathcal{D} \rightarrow \mathbb{R}$. A *random generalized function* X is a mapping such that, for every $\varphi \in \mathcal{D}$, the quantity $X(\varphi)$ is a real-valued random variable, and the map $\varphi \mapsto X(\varphi)$ is linear and continuous (in probability).

This formulation avoids pointwise evaluation and instead characterizes randomness through its action on test functions. Classical stochastic processes that fail to exist as functions—most notably Gaussian white noise—are naturally defined in this sense. For example, white noise W is characterized by

$$\mathbb{E}[W(\varphi)W(\psi)] = \langle \varphi, \psi \rangle_{L^2},$$

and therefore defines a centered Gaussian random generalized function.

Random generalized functions play a central role in stochastic partial differential equations, Gaussian processes with singular covariance kernels, and probabilistic models involving infinite-dimensional randomness, see (Da Prato & Zabczyk, 2014) to go further.

E. Proofs

E.1. Derivation of the coefficients \tilde{b} and $\tilde{\sigma}$

The derivation of the coefficients \tilde{b} and $\tilde{\sigma}$ follows from Germain & Monmarché (2025, Eq. 8). This formula, stated under the assumption that the observable can be expressed as a moment of the measure:

$$F(\mu) = \mu(f) := \int_{\mathbb{R}^d} f(x) d\mu(x) \quad (24)$$

with $f : \mathbb{R}^d \rightarrow \mathbb{R}^p$, gives the expression of \tilde{b} and $\tilde{\sigma}$ in terms of f , and of the coefficients a and s :

$$\begin{cases} \tilde{\sigma}_\mu(x) &= \nabla f(x) (\mu[\nabla f^T \nabla f])^{-1} s(\mu(f)) \\ \tilde{b}_\mu(x) &= \nabla f(x) (\mu[\nabla f^T \nabla f])^{-1} [a(\mu(f)) - \frac{1}{2} \mu(\tilde{\sigma}_\mu \tilde{\sigma}_\mu^T : \nabla^2 f)]. \end{cases} \quad (25)$$

where $\sigma_\mu \tilde{\sigma}_\mu^T : \nabla^2 f = (\sigma_\mu \tilde{\sigma}_\mu^T : \nabla^2 f_1, \dots, \sigma_\mu \tilde{\sigma}_\mu^T : \nabla^2 f_p)$ is a vector of \mathbb{R}^p , and $A : B$ represents the usual Hilbert-Schmidt scalar product between two matrices of $\mathbb{R}^{d \times d}$.

Because F_{mean} and $F_{s.m}$ directly fit this setting with:

$$f_{\text{mean}} : x \rightarrow x, \quad f_{s.m} : x \mapsto (x_1^2, \dots, x_d^2) \quad (26)$$

and respective coefficients $a_{\text{mean}} = 0$, $s_{\text{mean}} = I_d$, and $a_{s.o}(z) = [(\frac{\delta-1/2}{z_i})]_{i \in [d]}$, $s_{s.o} = I_d$

Equations Eq. 7 and Eq. 8 giving the expression of \tilde{b} and $\tilde{\sigma}$ for F_{mean} and $F_{s.m}$ follow from a direct explicit computation of equation Eq. 25.

Observables F_{var} and $F_{\text{mean+var}}$ do not directly fit this setting so one cannot directly compute equation \tilde{b} and $\tilde{\sigma}$ with Eq. 25. To do so, first assume that the particle system defined by equation Eq. 6 has its observable $F_{\text{mean+var}}(\hat{\rho}_{Y_t})$ satisfying the following SDE:

$$\begin{cases} dF_{\text{mean}}(\hat{\rho}_{Y_t}) &= \varepsilon dW_t^1 \\ dF_{\text{var}}(\hat{\rho}_{Y_t}) &= \frac{\delta-1}{F_{\text{var}}(\hat{\rho}_{Y_t})} dt + dW_t^2. \end{cases} \quad (27)$$

where W^1 and W^2 are two independent d dimensional Brownian motions and $\varepsilon \in [0, 1]$ corresponds respectively to the control of the Variance alone and of the mean and the variance. Again, the previous equation should be understood component by component since $F_{\text{var}}(\hat{\rho}_{Y_t}) \in \mathbb{R}^d$. Using the fact that $F_{\text{var}}(\hat{\rho}_{Y_t}) = F_{s.m}(\hat{\rho}_{Y_t}) - F_{\text{mean}}(\hat{\rho}_{Y_t})^2$, and that because of Itô's formula:

$$dF_{\text{mean}}(\hat{\rho}_{Y_t})^2 = 2\varepsilon F_{\text{mean}}(\hat{\rho}_{Y_t}) dW_t^1 + \varepsilon^2 dt$$

equation Eq. 27 rewrites as:

$$\begin{cases} dF_{\text{mean}}(\hat{\rho}_{Y_t}) &= \varepsilon dW_t^1 \\ dF_{s.m}(\hat{\rho}_{Y_t}) &= 2\varepsilon F_{\text{mean}}(\hat{\rho}_{Y_t}) dW_t^1 + \varepsilon^2 dt + \frac{\delta-1}{(F_{s.m}(\hat{\rho}_{Y_t}) - F_{\text{mean}}(\hat{\rho}_{Y_t}))^2} dt + dW_t^2. \end{cases} \quad (28)$$

which can be written as:

$$d\hat{\rho}_{Y_t}(f) = a(\hat{\rho}_{Y_t}(f))dt + s(\hat{\rho}_{Y_t}(f))dW_t \quad (29)$$

with $f = (f_{\text{mean}}, f_{s.m}) : \mathbb{R}^d \rightarrow \mathbb{R}^{2d}$, $W = (W^1, W^2)$ is a $2d$ dimensional Brownian process, and for $(z_1, z_2) \in \mathbb{R}^{2d}$:

$$a(z_1, z_2) = \begin{pmatrix} 0 \\ \frac{\delta+1}{2(z_2 - z_1^2)} + \varepsilon^2 \end{pmatrix}, \quad s(z_1, z_2) = \begin{pmatrix} \varepsilon & 0 \\ 2\varepsilon z_1 & 1 \end{pmatrix}$$

This formulation now fits the setting of equation Eq. 25, which can be computed explicitly. this finally gives:

$$\tilde{b}(x, \rho) = \left(\delta - \frac{3}{2} \right) \left[\frac{x - m(\rho)}{4 \text{Var}(\rho)^2} \right], \quad \tilde{\sigma}(x, \rho) = \left(\varepsilon I_d, \text{Diag} \left[\frac{x - m(\rho)}{2 \text{Var}(\rho)} \right] \right) \quad (30)$$

Taking $\varepsilon = 1$ gives the desired result for $F_{\text{mean+var}}$. Taking $\varepsilon = 0$ (which corresponds to a non perturbation of the mean of the system), and extracting the variance component gives the result for F_{var} .

E.2. Proof of Lemma 3.3

Proof. Let $X = (x_1, \dots, x_n) \in \mathbb{R}^{Nd}$ such that $x_i \neq x_j$ if $i \neq j$.

Define the evaluation map

$$\text{Ev}_X : \mathcal{H}_d \rightarrow \mathbb{R}^{Nd}, \quad \text{Ev}_X(f) := (f(x_1), \dots, f(x_N)),$$

where $f(x_i) \in \mathbb{R}^d$ and the concatenation is in \mathbb{R}^{Nd} .

Restriction of Ev_X to \mathcal{H}_d^X is an isomorphism. Consider the restriction $\text{Ev}_X : \mathcal{H}_d^X \rightarrow \mathbb{R}^{Nd}$. First, Ev_X is injective on \mathcal{H}_d^X . Indeed, let $f \in \mathcal{H}_d^X$ and assume $\text{Ev}_X(f) = 0$. Write $f(\cdot) = \sum_{i=1}^N K(x_i, \cdot) c_i$ for some $c = (c_1, \dots, c_N) \in \mathbb{R}^{Nd}$ with $c_i \in \mathbb{R}^d$. Then for each $l \in [N]$:

$$0 = f(x_l) = \sum_{i=1}^N K(x_i, x_l) c_i,$$

which in block form reads $(K_X \otimes I_d)c = \bar{K}c = 0$. Because K is strictly positive definite and the points (x_i) are distinct, then K_X is invertible, hence \bar{K} is invertible and $c = 0$, so $f = 0$. Thus Ev_X is injective.

Since $\dim(\mathcal{H}_d^X) \leq Nd$ and the family $\{K(x_i, \cdot)e_j\}$ spans \mathcal{H}_d^X , we have $\dim(\mathcal{H}_d^X) = Nd$. Therefore Ev_X is bijective. In particular, for any $g = (g_1, \dots, g_N) \in \mathbb{R}^{Nd}$ with $g_i \in \mathbb{R}^d$, there exists a unique $f \in \mathcal{H}_d^X$ such that $f(X) = g$, namely

$$f(\cdot) = \sum_{i=1}^N K(x_i, \cdot) c_i, \quad c = (K_X^{-1} \otimes I_d)g = \bar{K}^{-1}g. \quad (31)$$

Isometry after equipping \mathbb{R}^{Nd} with the kernel-induced norm. Define on \mathbb{R}^{Nd} the inner product

$$\langle g, h \rangle_{\bar{K}^{-1}} := g^\top \bar{K}^{-1} h, \quad \|g\|_{\bar{K}^{-1}}^2 := g^\top \bar{K}^{-1} g.$$

Then $\text{Ev}_X : \mathcal{H}_d^X \rightarrow (\mathbb{R}^{Nd}, \langle \cdot, \cdot \rangle_{\bar{K}^{-1}})$ is an isometry. Indeed, let $f \in \mathcal{H}_d^X$ and write $f = \sum_i K(x_i, \cdot) c_i$. Using the product structure of \mathcal{H}_d and the reproducing kernel calculus,

$$\|f\|_{\mathcal{H}_d}^2 = \left\langle \sum_i K(x_i, \cdot) c_i, \sum_\ell K(x_\ell, \cdot) c_\ell \right\rangle_{\mathcal{H}_d} = \sum_{i, \ell} c_i^\top c_\ell K(x_i, x_\ell) = c^\top (K_X \otimes I_d) c = c^\top \bar{K} c.$$

On the other hand $g := f(X) = \bar{K} c$, hence $c = \bar{K}^{-1} g$, and therefore

$$\|f\|_{\mathcal{H}_d}^2 = (\bar{K}^{-1} g)^\top \bar{K} (\bar{K}^{-1} g) = g^\top \bar{K}^{-1} g = \|g\|_{\bar{K}^{-1}}^2. \quad (32)$$

This proves that $\|f\|_{\mathcal{H}_d} = \|\text{Ev}_X(f)\|_{\bar{K}^{-1}}$ for all $f \in \mathcal{H}_d^X$.

Reference (Lebesgue) measure on \mathcal{H}_d^X . Since \mathcal{H}_d^X is a finite-dimensional Hilbert space, the inner product $\langle \cdot, \cdot \rangle_{\mathcal{H}_d}$ induces a canonical volume measure, defined as the Lebesgue measure in any orthonormal coordinate system. Concretely, choose an orthonormal basis (u_1, \dots, u_{Nd}) of \mathcal{H}_d^X and define, for Borel sets $A \subset \mathcal{H}_d^X$,

$$\mu_{\mathcal{H}_d^X}(A) := \lambda_{Nd}(\Phi(A)), \quad \Phi(f) := (\langle f, u_1 \rangle_{\mathcal{H}_d}, \dots, \langle f, u_{Nd} \rangle_{\mathcal{H}_d}),$$

where λ_{Nd} is the usual Lebesgue measure on \mathbb{R}^{Nd} . This definition does not depend on the chosen orthonormal basis. Equivalently, using the isometry Eq. 32, $\mu_{\mathcal{H}_d^X}$ is the pullback by Ev_X of the Lebesgue measure on \mathbb{R}^{Nd} associated with the inner product $\langle \cdot, \cdot \rangle_{\bar{K}^{-1}}$, i.e.

$$\mu_{\mathcal{H}_d^X} = (\text{Ev}_X)_\#^{-1} \lambda_{\bar{K}^{-1}},$$

where $\lambda_{\bar{K}^{-1}}$ denotes the Lebesgue measure on \mathbb{R}^{Nd} in an orthonormal basis for $\langle \cdot, \cdot \rangle_{\bar{K}^{-1}}$. In standard Euclidean coordinates $g \in \mathbb{R}^{Nd}$, one has

$$d\lambda_{\bar{K}^{-1}}(g) = (\det \bar{K})^{-1/2} dg,$$

since an orthonormalization amounts to the linear change of variables $z = \bar{K}^{-1/2} g$.

Finite-dimensional Gaussian density (proof of Lemma). Let $G(X) \sim \mathcal{N}(0, \bar{K})$. Its density with respect to the standard Lebesgue measure dg on \mathbb{R}^{Nd} is

$$p_{G(X)}(g) = \frac{1}{(2\pi)^{Nd/2} (\det \bar{K})^{1/2}} \exp\left(-\frac{1}{2} g^\top \bar{K}^{-1} g\right).$$

By Eq. 32, for $f \in \mathcal{H}_d^X$ and $g = \text{Ev}_X(f)$, $g^\top \bar{K}^{-1} g = \|f\|_{\mathcal{H}_d}^2$. Moreover, since Ev_X is an isometry between \mathcal{H}_d^X and $(\mathbb{R}^{Nd}, \langle \cdot, \cdot \rangle_{\bar{K}^{-1}})$, the change-of-variables formula yields

$$\mathbb{P}(\pi_X G \in df) = p_{G(X)}(\text{Ev}_X(f)) d\lambda_{\bar{K}^{-1}}(\text{Ev}_X(f)) \propto \exp\left(-\frac{1}{2} \|f\|_{\mathcal{H}_d}^2\right) d\mu_{\mathcal{H}_d^X}(f),$$

which is the claimed statement. □

E.3. Proof of Lemma 3.5

Start from the following equation:

$$\hat{\rho}_{(n+1)\varepsilon} = (id + \varepsilon v_{n\varepsilon} + \sqrt{\varepsilon} G_n) \# \hat{\rho}_{n\varepsilon}, \quad G_n \sim \mathcal{G}(\beta^2 K_{SVGD}) \quad (33)$$

This equation can be interpreted as a noisy version of the discretized in time continuity equation for the SVGD metric.

$$\partial_t \rho_t + \nabla \cdot (\rho_t v_t) = 0$$

As it is classical within PDE theory, evolutions of this type are usually discretized in space thanks to the use of particle systems. First approximate $\hat{\rho}_0$ by the empirical distribution of a particle system $\bar{\rho}_0^\varepsilon := \frac{1}{N} \sum_{i=1}^N \delta_{X_0^{\varepsilon, i}}$. Then, the iteration Eq. 33 initialized with $\bar{\rho}_0$ rewrites as an iteration on the particles:

$$X_{n+1}^{\varepsilon, i} = \varepsilon v_n(X_n^{\varepsilon, i}) + \sqrt{\varepsilon} G_n(X_n^{\varepsilon, i}) \quad (34)$$

The iteration Eq. 33 initialized with $\hat{\rho}_0$ is then approximated with:

$$\hat{\rho}_{n\varepsilon} \approx \bar{\rho}_{n\varepsilon} = \frac{1}{N} \sum_{i=1}^N \delta_{X_n^{\varepsilon, i}}$$

We now want to derive a continuous time version of Eq. 34, obtained when $\varepsilon \rightarrow 0$. To do so, remark that the vector $G_n(X_n^\varepsilon) := (G_n(X_n^{\varepsilon, 1}), \dots, G_n(X_n^{\varepsilon, N})) \in \mathbb{R}^{Nd}$ is Gaussian, and its covariance matrix is given by:

$$C_\beta(X_n^\varepsilon) = \beta^2 \bar{K}(X_n^\varepsilon), \quad K(X_n^\varepsilon) = \begin{pmatrix} K_{1,1} & \cdots & K_{1,N} \\ \vdots & \ddots & \vdots \\ K_{N,1} & \cdots & K_{N,N} \end{pmatrix}, \quad K_{i,j} = k(x_i, x_j) I_d.$$

which can be reformulated as :

$$\bar{K}(X) = K(X) \otimes I_d, \quad K(X)_{i,j} = k(X^i, X^j) \quad (35)$$

Then, using the theory of Gaussian vectors, Eq. 34 can be expressed in a matrix form by:

$$X_{n+1}^\varepsilon = \varepsilon v_n(X_n^\varepsilon) + \sqrt{\varepsilon \beta^2 \bar{K}(X_n^\varepsilon)} \xi_{n+1} \quad (36)$$

where $(\xi_n)_{n \in \mathbb{N}}$ are i.i.d standard Gaussian variables of dimension Nd .

One can identify equation Eq. 36 as Euler-Maruyama discretization of the following SDE:

$$dX_t = v_t(X_t) dt + \beta \sqrt{\bar{K}(X_t)} dB_t \quad (37)$$

The equations Eq. 37, Eq. 34 and Eq. 36 correspond respectively to the continuous in time/ discretized in space; continuous in space/ discretized in time and discretized in time/ discretized in space version of the underlying continuous in time/ continuous in space dynamic Eq. 20.

E.4. Proof of Theorem 3.7

Proof. We have that for any $X \in \mathbb{R}^{Nd}$, $K_X \rightarrow \bar{J}$ where $\bar{J} = J \otimes I_d$ where $J = (1)_{i,j \in [N^2]}$ is the matrix with only 1 values, thus $K_X^{1/2} \rightarrow \bar{J}/\sqrt{N}$ since $\bar{J}^2 = N\bar{J}$. Therefore in the case $\sigma \rightarrow \infty$, we have $k_\sigma(x, y) = 1$, then by Eq. 19, $\bar{G}_t^N = (\sum_{i=1}^N B_t^i / \sqrt{N})_{j \in [N]}$ meaning that $G_t(X_j^N) = Z$ for any $j \in [N]$ with $Z \sim \mathcal{N}(0, I_d)$. In other words, when $\sigma \rightarrow \infty$, GCN is SMD-mean.

In the case, $\sigma \rightarrow 0$, $k_\sigma(x, y)^{(d)} \rightarrow \delta_0(x - y)$, meaning that $G \sim \mathcal{G}(k)$ satisfies $\mathbb{E}(G(x)G(y)) = \delta_0(x - y)$ which defines a white noise. \square

E.5. Proof of Theorem 3.6

We take the same starting point as the proof of Proposition 2 in (Duncan et al., 2023). Let $\varphi \in C_c^\infty([0, \infty) \times \mathbb{R}^d)$ be a smooth test function with compact support and define $\Phi \in C_c^\infty([0, \infty) \times \mathbb{R}^{Nd})$ by $\Phi(t, x) := \frac{1}{N} \sum_{i=1}^N \varphi(t, x_i)$ for any $x = (x_1, \dots, x_N) \in \mathbb{R}^{Nd}$. Denoting by for any $\tilde{x} \in \mathbb{R}^d$ and $\rho \in \mathcal{P}(\mathbb{R}^d)$,

$$b(\tilde{x}, \rho) = \mathbb{E}_{X \sim \rho} \left[-k(\tilde{x}, X) \nabla V(X) + \nabla_x k(\tilde{x}, X) \right] = \int_{\mathbb{R}^d} [-k(\tilde{x}, y) \nabla V(y) + \nabla_y k(\tilde{x}, y)] d\rho(y)$$

Let $(\bar{X}_t)_{t \geq 0}$ a solution of Eq. 18, Itô's formula implies

$$\begin{aligned} d\Phi(t, \bar{X}_t) &= \frac{1}{N} \sum_{i=1}^N (\partial_t \varphi(t, X_t^i) + \nabla \varphi(t, X_t^i) \cdot b(X_t^i, \rho_t^N)) dt + \beta^2 \operatorname{Tr}(\bar{K}_{\bar{X}_t} \operatorname{Hess} \Phi(t, \bar{X}_t)) dt \\ &\quad + \frac{\beta}{N} \sum_{i,j=1}^N \nabla \varphi(t, X_t^i) \cdot \left[\sqrt{\bar{K}_{\bar{X}_t}} \right]_{ij} dW_t^j \end{aligned}$$

where $\left[\sqrt{\bar{K}_{\bar{X}_t}} \right]_{ij} \in \mathbb{R}^{d \times d}$ is the matrix block in line i and column j in $\sqrt{\bar{K}_{\bar{X}_t}}$ and $(W_t = (W_t^1, \dots, W_t^N))_{t \geq 0}$ is a Nd -dimensional Brownian motion. The Hessian $\operatorname{Hess} \Phi \in \mathbb{R}^{Nd \times Nd}$ consists of N^2 blocks of size $d \times d$ with

$$[\operatorname{Hess} \Phi(t, x)]_{ij} = \begin{cases} \frac{1}{N} \operatorname{Hess} \varphi(t, x_i) & \text{if } i = j \\ 0 & \text{otherwise} \end{cases}, \quad (i, j) \in \{1, \dots, N\}^2$$

so that it is a block diagonal matrix, with each diagonal block containing the Hessian of φ . A simple calculation yields that

$$\operatorname{Tr}(\bar{K}_x \operatorname{Hess} \Phi(t, x)) = \frac{1}{N} \sum_{i=1}^N k(x_i, x_i) \operatorname{Tr}(\operatorname{Hess} \varphi(t, x_i)) = \frac{1}{N} \sum_{i=1}^N k(x_i, x_i) \Delta_{x_i} \varphi(t, x_i),$$

so that

$$\operatorname{Tr}(\mathcal{K}(\bar{X}_t) \operatorname{Hess} \Phi(t, \bar{X}_t)) = \int_{\mathbb{R}^d} k(x, x) \Delta_x \varphi(t, x) d\rho_t^N(x)$$

Denoting by $\rho_s^N = \sum_{i=1}^N \delta_{X_s^i}/N$, it follows that

$$\begin{aligned} \langle \varphi(t, \cdot), \rho_t^N \rangle - \langle \varphi(0, \cdot), \rho_0^N \rangle &= \int_0^t \langle \partial_s \varphi(s, \cdot), \rho_s^N \rangle ds + \int_0^t \langle \nabla \varphi(s, \cdot) \cdot b(\cdot, \rho_s^N), \rho_s^N \rangle ds \\ &\quad + \beta^2 \int_0^t \langle k(\cdot, \cdot) \Delta_x \varphi(s, \cdot), \rho_s^N \rangle ds + \beta \mathcal{N}_t \end{aligned}$$

where the brackets denote the duality pairing between test functions and measures. The term \mathcal{N}_t represents a local martingale with quadratic variation

$$\begin{aligned} [\mathcal{N} \cdot, \mathcal{N} \cdot]_t &= \frac{1}{N^2} \int_0^t \sum_{i,j=1}^N \nabla \varphi(s, X_s^i) \cdot \mathcal{K}(\bar{X}_s)_{ij} \nabla \varphi(s, X_s^j) ds \\ &= \frac{1}{N^2} \int_0^t \sum_{i,j=1}^N \nabla \varphi(s, X_s^i) \cdot \nabla \varphi(s, X_s^j) k(X_s^i, X_s^j) ds \\ &= \int_0^t \int_{\mathbb{R}^d} \int_{\mathbb{R}^d} \nabla \varphi(s, y) \cdot \nabla \varphi(s, z) k(y, z) d\rho_s^N(y) d\rho_s^N(z) ds \end{aligned}$$

In particular, assuming that the family $\{\rho_s^N : N \in \mathbb{N}\}$ possesses a limit point in $\mathcal{P}(C[0, T])$ denoted by ρ_s^* , it follows that

$$[\mathcal{N}^* \cdot, \mathcal{N}^* \cdot]_t = \int_0^t \int_{\mathbb{R}^d} \int_{\mathbb{R}^d} \nabla \varphi(s, y) \cdot \nabla \varphi(s, z) k(y, z) d\rho_s^*(y) d\rho_s^*(z) ds.$$

\mathcal{N}^* is uniquely defined by its quadratic variation, such that we have

$$\mathcal{N}_t^* = \int_0^t \langle \nabla \varphi(s, \cdot) \cdot dG(s, \cdot), \rho_s^* \rangle \quad (38)$$

where $G \sim \mathcal{T}\mathcal{G}(K_{\text{SVGD}})$. At the limit,

$$\begin{aligned} \langle \varphi(t, \cdot), \rho_t^* \rangle - \langle \varphi(0, \cdot), \rho_0^* \rangle &= \int_0^t \langle \partial_s \varphi(s, \cdot), \rho_s^* \rangle \, ds + \int_0^t \langle \nabla \varphi(s, \cdot) \cdot b(\cdot, \rho_s^*), \rho_s^* \rangle \, ds \\ &\quad + \beta^2 \int_0^t \langle k(\cdot, \cdot) \Delta_x \varphi(s, \cdot), \rho_s^* \rangle \, ds + \beta \mathcal{N}_t^* \end{aligned}$$

ρ_s^* is thus solution of the following equation in the weak sense

$$\partial_t \rho_s^* + \text{div}((b(\cdot, \rho_s^*) + \beta \text{d}G(s, \cdot)) \rho_s^*) + \beta^2 \Delta_s(k(\cdot, \cdot) \rho_s^*) = 0, \quad G \sim \mathcal{T}\mathcal{G}(K_{\text{SVGD}}) \quad (39)$$

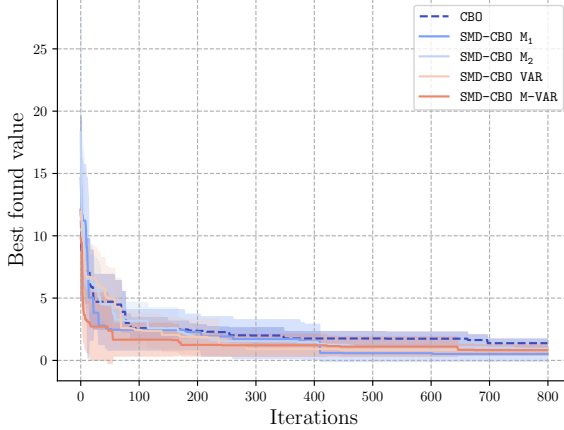
This concludes the proof for Eq. 20.

Regarding Eq. 21, the proof proceeds from the following computation

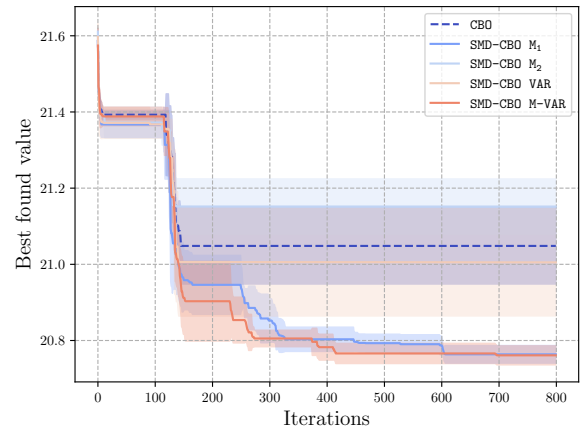
$$\int_0^\varepsilon \text{d}G_i(s, \cdot) = \sum_{\vec{n} \in \mathbb{N}^d} \int_0^\varepsilon \lambda_{\vec{n}} \varphi_{\vec{n}} \text{d}\xi_{\vec{n}, t}^i = \sum_{\vec{n} \in \mathbb{N}^d} \lambda_{\vec{n}} \varphi_{\vec{n}} \int_0^\varepsilon \text{d}\xi_{\vec{n}, t}^i = \sqrt{\varepsilon} \sum_{\vec{n} \in \mathbb{N}^d} \lambda_{\vec{n}} \varphi_{\vec{n}} \xi_{\vec{n}}^i = \sqrt{\varepsilon} g, \quad \xi_{\vec{n}}^i \stackrel{i.i.d.}{\sim} \mathcal{N}(0, 1) \quad (40)$$

where $g \sim \mathcal{G}(K_{\text{SVGD}})$ by Remark 3.4 and by Eq. 13.

F. Additional Numerical Experiments



(a) Impact of SMD on CBO dynamics on Rastrigin function in dimension 2 with 10 particles.



(b) Impact of SMD on CBO dynamics on Ackley function in dimension 200 with 10 particles.

Figure 3. Illustration of the problem-dependent effects of noise injection methods in the multimodal setting. The mean (line) and standard deviation (shaded area) of the best found value are reported over 5 runs. In low dimension with sufficient particles (left), the effect of SMD is negligible, while in very high dimension with scarce particles (right), SMD yields modest improvements.

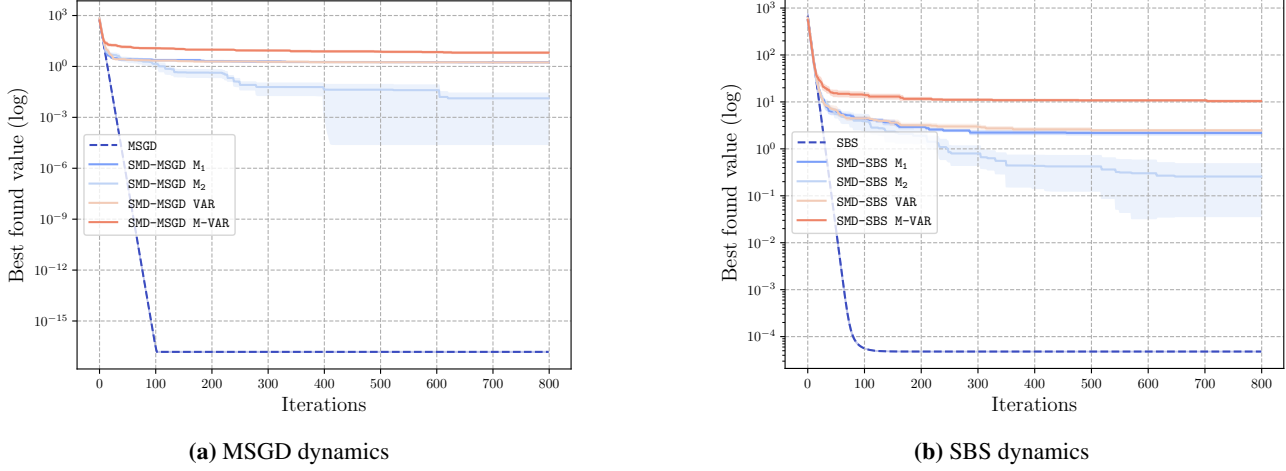


Figure 4. Impact of perturbed observables on MSGD (left) and SBS dynamics (right) on the Square function in dimension 20 with 2 particles. The mean (line) and standard deviation (shaded area) of the best found value are reported over 5 runs. In this unimodal setting, the noise injection slightly degrades performance by introducing unnecessary perturbations.

Table 2. Comparison between vanilla dynamics and their SMD and GCN variants on 8 unimodal benchmark functions in dimension 20 using 150 particles over 300 iterations. For each dynamic, the average best result is reported. The average rank over all benchmarks along with the ECR is reported at the bottom of each table. The maximum p-value of Mann-Whitney U tests is reported in the last column. The best results are in bold and cells where the Mann-Whitney U test is significant at level 0.05 are highlighted in gray.

	CBO	SMD-CBO Mean	SMD-CBO M ²	SMD-CBO Var	SMD-CBO Mean+Var	GCN-CBO	p-value
Bent cigar	30623584067.892	29682175177.256	31818328261.401	31057209405.099	30240038880.044	30457405283.166	0.281
Dixon-Price	469983.927	371918.118	442706.838	461788.187	380525.484	378987.734	0.000
Hyper-Ellipsoid	814.670	714.377	806.037	765.882	734.561	729.761	0.000
Rosenbrock	488088.345	378862.224	498337.068	473975.528	371117.547	351728.228	0.000
Square	336.981	306.784	335.871	317.282	304.169	301.648	0.001
Sumpow	41.136	9.806	34.587	30.481	10.263	10.263	0.000
Trid	-0.005	-0.006	-0.005	-0.004	-0.005	-0.006	0.022
Zakharov	635.966	585.580	664.924	597.844	605.961	606.866	0.011
Avg Rank	5.25	1.62	5.25	4.25	2.50	2.12	
ECR	1.5283	1.0119	1.4488	1.3621	1.0271	1.0187	

	SBS	SMD-SBS Mean	SMD-SBS M ²	SMD-SBS Var	SMD-SBS Mean+Var	GCN-SBS	p-value
Bent cigar	32005162588.056	31363252573.409	31743875639.769	31890761748.545	31987545635.464	31146357732.286	0.206
Dixon-Price	444531.288	438354.660	455444.623	459341.343	434068.195	456453.507	0.627
Hyper-Ellipsoid	2.230	202.142	2.725	5.652	207.690	130.216	0.570
Rosenbrock	444772.184	453814.436	513107.614	487215.524	463959.093	502791.601	0.879
Square	153.365	193.608	152.775	152.288	175.262	175.231	0.975
Sumpow	0.260	1.743	0.002	7e-4	0.039	0.160	0.000
Trid	0.004	0.001	0.002	0.002	0.001	-8e-5	0.000
Zakharov	1018737.046	450180.203	378128.839	612121.643	734513.842	62513.402	0.293
Avg Rank	3.88	3.62	3.25	3.38	3.75	3.12	
ECR	15.2971	25.3978	1.8410	2.3145	20.2180	20.5921	

	Langevin	SMD-Langevin Mean	SMD-Langevin M ²	SMD-Langevin Var	SMD-Langevin Mean+Var	GCN-Langevin	p-value
Bent cigar	32535447108.573	31621953123.250	32072428247.128	31976284652.507	32565581749.156	31819674299.149	0.224
Dixon-Price	451898.516	454002.991	468710.179	460187.324	443581.877	481332.550	0.603
Hyper-Ellipsoid	828.543	825.205	779.643	798.520	812.076	803.315	0.033
Rosenbrock	490079.993	459736.311	482284.302	464262.042	493496.166	494916.053	0.372
Square	0.979	1.877	1.376	1.367	2.545	1.979	0.000
Sumpow	6e-5	3e-5	1e-4	1e-6	2e-5	5e-5	0.000
Trid	-2e-4	1e-4	-5e-4	-2e-4	-3e-4	-7e-4	0.038
Zakharov	109659.961	544154.097	406593.891	394359.838	920400.543	788568.950	1.000
Avg Rank	3.62	3.38	3.38	2.50	4.12	4.00	
ECR	6.2152	4.4340	10.4760	1.3848	4.3054	6.5461	

	MSGD	SMD-MSGD Mean	SMD-MSGD M ²	SMD-MSGD Var	SMD-MSGD Mean+Var	GCN-MSGD	p-value
Bent cigar	31678046302.237	31462840710.309	31473260670.919	32549106519.774	32133802466.087	30786379896.381	0.216
Dixon-Price	440543.067	453061.646	459649.761	444971.192	450100.101	453917.746	1.000
Hyper-Ellipsoid	794.589	785.260	798.768	789.540	801.574	773.490	0.471
Rosenbrock	501435.007	474768.154	458605.030	481823.429	470479.892	480760.075	0.155
Square	3e-18	1.789	5e-11	0.005	1.549	1.000	0.000
Sumpow	3e-5	0.012	0	0	0	9e-5	0.000
Trid	0.003	0.001	0.002	0.002	9e-4	-3e-4	0.000
Zakharov	555551.173	253587.981	508868.077	395610.144	306451.213	450211.111	0.030
Avg Rank	4.00	3.38	3.50	3.38	3.25	3.12	
ECR	13.5453	25.7640	1.2142	13.4638	13.4180	25.8568	